Nanotechnology **19** (2008) 015606 (6pp) doi:10.1088/0957-4484/19/01/015606

High-yield synthesis and optical response of gold nanostars

Pandian Senthil Kumar[1], **Isabel Pastoriza-Santos**[1], **Benito Rodríguez-González**[1], **F Javier García de Abajo**[2] and **Luis M Liz-Marzán**[1]

[1] Departamento de Química Física and Unidad Asociada CSIC-Universidade de Vigo, 36310 Vigo, Spain
[2] Instituto de Óptica–CSIC, Serrano 121, 28006 Madrid, Spain

E-mail: jga@io.cfmac.csic.es and lmarzan@uvigo.es

Received 1 August 2007, in final form 15 October 2007
Published 29 November 2007
Online at stacks.iop.org/Nano/19/015606

Abstract
Multipod Au nanoparticles (nanostars) with single crystalline tips were synthesized in extremely high yield through the reduction of $HAuCl_4$ in a concentrated solution of poly(vinylpyrrolidone) (PVP) in *N*,*N*-dimethylformamide (DMF), in the presence of preformed Au nanoparticle seeds, but with no need for external energy sources. Nanostar dispersions display a well-defined optical response, which was found (through theoretical modeling) to comprise a main mode confined within the tips and a secondary mode confined in the central body. Calculations of the surface enhanced Raman scattering (SERS) response additionally show that this morphology will be relevant for sensing applications.

S Supplementary data are available from stacks.iop.org/Nano/19/015606

1. Introduction

The optical properties of metal nanoparticles are of great importance for applications in the fields of photonics, electronics, sensing, and various other biomedical uses. It has been demonstrated that the presence of sharp edges and tips provides a very high sensitivity to local changes in the dielectric environment, as well as larger enhancements of the electric field around the nanoparticles [1]. These features constitute the basis of localized surface plasmon resonance (LSPR) or surface enhanced Raman scattering (SERS) analyses [1]. For this reason, an increasing number of synthetic procedures are being developed, aiming at a simultaneous control of the size and shape of the metal nanoparticles, among which the production of gold nanospheres, nanorods, or even nanoplatelets with a certain degree of control of the size/shape distribution can almost be considered as routine experiments [2]. Other more sophisticated geometries have been seldom reported and are often limited by a low yield of the morphology of interest, by a poor control of particle size and high polydispersity, or by ill-defined properties [3–7].

We report in this paper a simple strategy for the controlled synthesis of branched Au nanoparticles with well-defined optical response, showing two resonance modes, which are assigned as localized within the central part and the tips of such particles, respectively, showing a good potential for future SERS and biosensing applications.

2. Experimental details

2.1. Materials and methods

In a typical synthesis, 82 μl of an aqueous solution of 50 mM chloroauric acid ($HAuCl_4$, Aldrich) was mixed with 15 ml of 10 mM, 5 mM or 2.5 mM poly(vinylpyrrolidone) (PVP, average MW = 10 000 or 24 000, Fluka) solution in *N*,*N*-dimethylformamide (DMF, Fluka), followed by rapid addition of 43 μl of a preformed dispersion of 15 nm, PVP-coated Au seeds [8] in ethanol ([Au] = 4.2 mM) under stirring. Within 15 min, the color of the solution changes from pink to colorless, and it finally turns blue, indicating the formation of gold nanostars in solution. All experiments were carried out at room temperature and all chemicals were used as received.

2.2. Characterization

A JEOL JEM 1010 transmission electron microscope (TEM) operating at an accelerating voltage of 100 kV was used for low

magnification imaging, while high resolution TEM (HRTEM) images were obtained using a JEOL JEM 2010 FEG-TEM operating at an acceleration voltage of 200 kV. For TEM measurements, the samples were centrifuged (3500 rpm) and redispersed in ethanol at least five times, so as to remove excess PVP, which otherwise makes TEM observation very complicated. UV–vis spectra were measured with an Agilent 8453 UV–vis–NIR diode-array spectrophotometer.

2.3. Optical modeling

Simulations of optical spectra and near-field enhancement maps were obtained using the boundary element method (BEM) [9]. In the BEM, the electromagnetic fields are expressed in terms of surface integrals involving charge (σ_j) and current ($\boldsymbol{h}_j$) distributions defined on the boundary of each region j. In our case, j runs over media representing gold (described by its measured frequency-dependent dielectric function taken from [10]), and DMF (described by an index of refraction of 1.428 as measured with an ABBE refractometer). The boundary conditions of the electromagnetic fields are then imposed to yield a set of self-consistent surface integral equations that determine the surface sources and that are recast into a linear set of equations by discretizing the surface through a finite number of representative boundary points. These equations are solved in turn by linear algebra techniques. The particles were described by axially symmetric shapes capturing the main physical aspects of their response to external illumination. The BEM is particularly advantageous in axial symmetry, where each azimuthal component m, involving fields that depend on the azimuthal angle ϕ as $e^{im\phi}$, is uncoupled from the rest of the components. Then, the surface of the particle can be parameterized with a contour line, thus reducing the problem effectively to one dimension. We have assimilated the stars to a central sphere of radius a with either one or two (located at opposite sides of the sphere) pseudo-conical caps of length L, radius of tip curvature s, and tip half-angle aperture α. Convergence has been achieved with 150 parameterization points.

3. Results and discussion

Recently, we have reported the uniform growth of gold decahedra and octahedra with controlled size and shape and well-characterized optical properties [11]. This synthetic procedure was based on the well-known reducing ability of *N*,*N*-dimethylformamide (DMF) [12], in combination with poly(vinylpyrrolidone) (PVP), as a stabilizer, using ultrasound as an energy source and preformed nanoparticle seeds as catalysts.

Although an external energy source is required for Au reduction when the PVP concentration is low, the use of considerably larger PVP concentrations (see section 2) has been found to lead to the reproducible synthesis of star-like, multipod nanoparticles in a very simple way. The yield of branched particles is extremely high (practically 100%), as demonstrated by TEM observation, where no other shapes were found in any of the analyzed samples (figure 1). The size

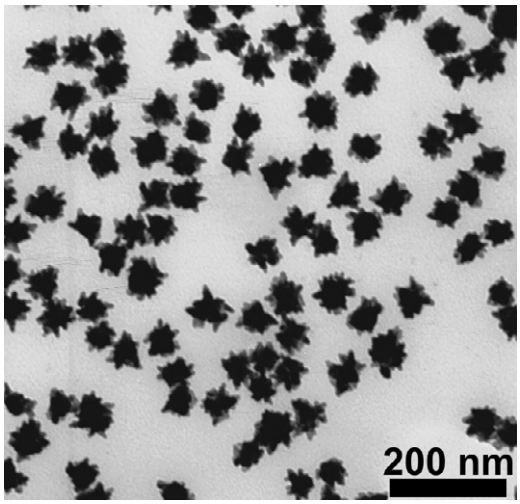

Figure 1. Representative transmission electron microscopy (TEM) image of Au nanostars synthesized through reduction of $HAuCl_4$ in a PVP/DMF mixture, in the presence of preformed Au seeds, using 10 mM PVP (Mw = 24 000).

distribution is wide when reduction is carried out directly from the gold salt, but becomes rather narrow when preformed Au seeds are added (see the size distribution in figure S1 (available at stacks.iop.org/Nano/19/015606) and a TEM image of the seeds in figure S2 (available at stacks.iop.org/Nano/19/015606) for comparison).

The key factor in our present case is likely to be connected with the reducing effect of PVP molecules in DMF, which additionally controls the reduction kinetics of $AuCl_4^-$ ions on the surface of preformed Au seeds. A strong argument in favor of the fundamental role of PVP is found when an intermediate PVP concentration is used (2.5 mM), leading to much more uniform particle growth compared to the larger concentrations (5 and 10 mM) (figure 2). It should be noted that these concentrations are equivalent to molar ratios of vinylpyrrolidone monomeric units to Au atoms as large as 800, 1640, and 3250, respectively. Therefore, we propose a rapid, kinetically controlled, preferential growth along various crystal faces facilitated by sequential interaction through adsorption/desorption processes [13], enabling them to grow in the shape of stable star/flower-like, multipod Au nanostructures, a drastically different morphology as compared with particles previously synthesized using PVP or other surfactants [14, 15]. As shown in figures 1 and 2 (see also figures S3, S4 in SI (available at stacks.iop.org/Nano/19/015606)), the shapes of all the nanoparticles prepared with high PVP concentration resemble a star/flower-like assembly with all rays/petals radially grown outwards from a common center and ending as rather sharp tips.

The crystalline structure of these nanostars was investigated using a high resolution transmission electron microscope (HRTEM, JEOL 2010F). Figure 3 shows TEM images (in bright and dark field) of a single flower-like nanoparticle, along with the corresponding selected area electron diffraction (SAED) pattern, indexed to a polycrystalline gold fcc crystal structure. It is indeed noteworthy that several clustered

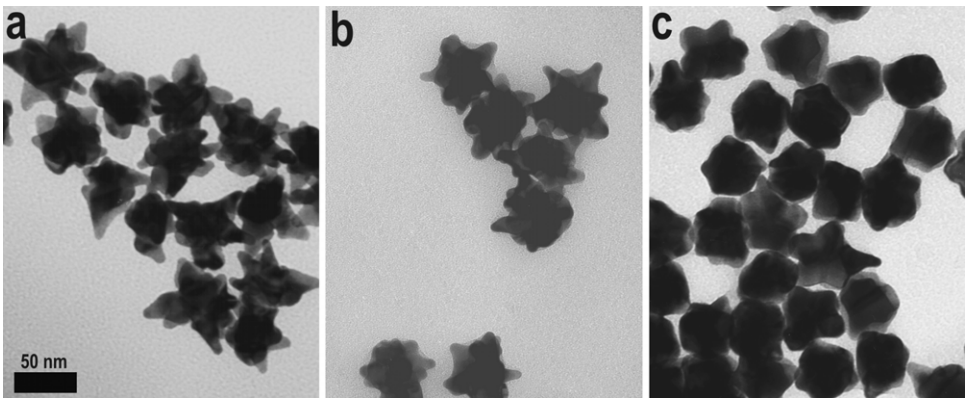

Figure 2. TEM images of Au nanostars synthesized through reduction of $HAuCl_4$ in a PVP/DMF mixture, in the presence of preformed Au seeds, using different PVP (Mw = 10 000) concentrations: 10.0 (a), 5.0 (b), and 2.5 mM (c).

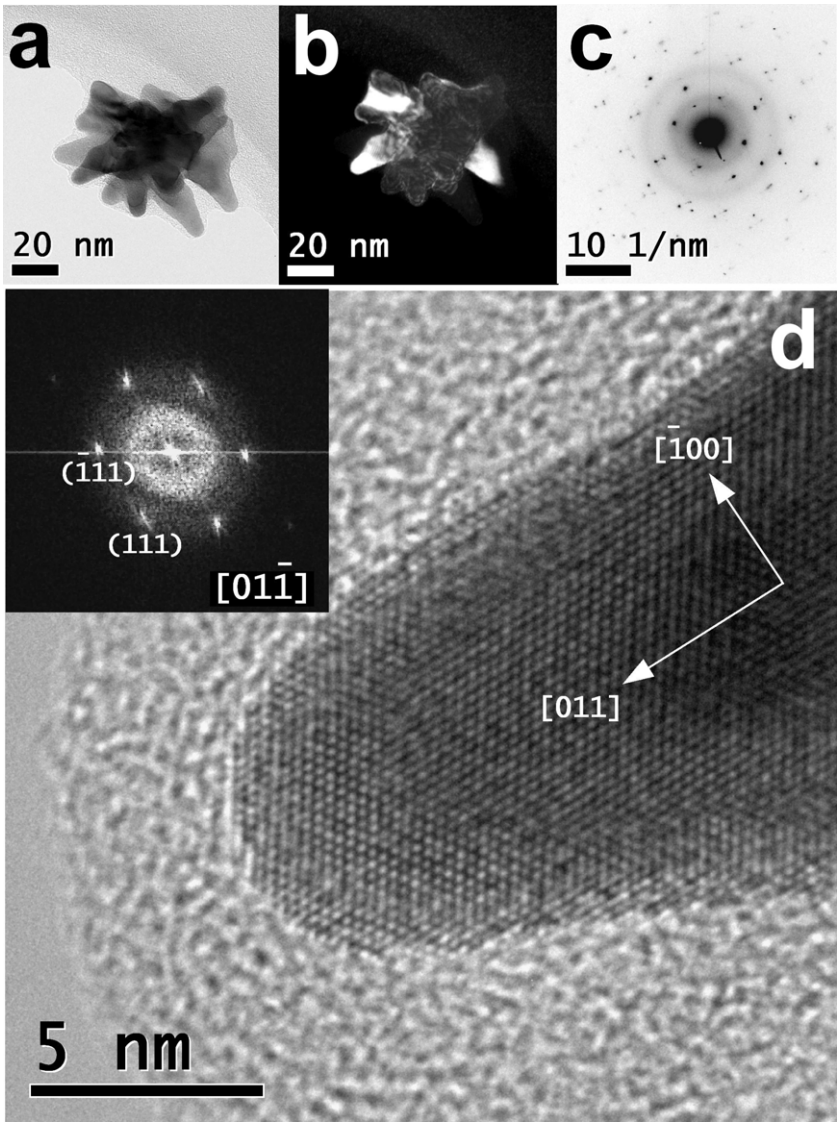

Figure 3. Top: bright field (a) and dark field (b) TEM images of a single nanostar, along with its corresponding SAED pattern (c). Bottom: HRTEM image of one single tip in the nanostar where the [011] growth direction of the tip can be clearly identified (the inset is the corresponding FFT pattern, demonstrating that the image in (d) was obtained in the $[01\bar{1}]$ zone axis).

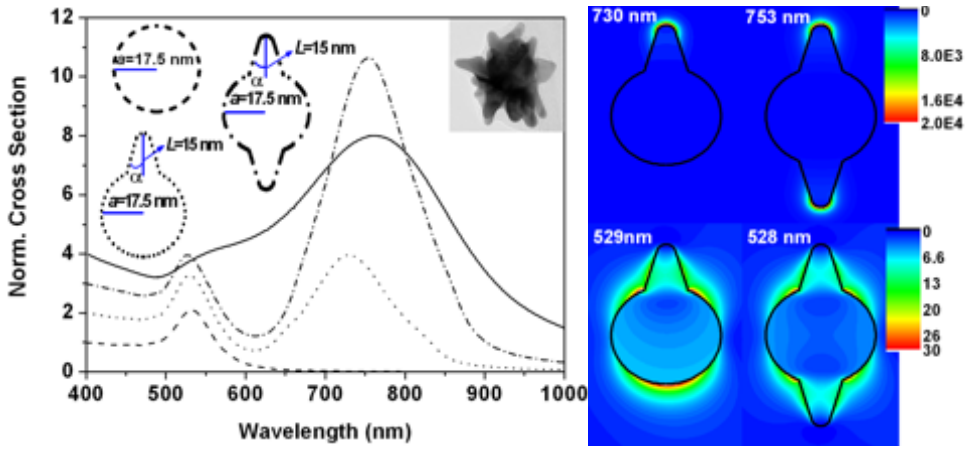

Figure 4. Left: experimental (solid line) and BEM calculated absorption spectra for Au nanostars, averaged over the measured distribution of tip-aperture angles α (broken curves). The morphologies corresponding to the various calculations are graphically depicted along with a TEM image. Right: calculated near-field enhancement ($|E/E_{\text{incident}}|^2$) maps for spheres with one and two tips at wavelengths of band maxima (see labels). The dimensions used for the simulations of the near-fields were $L = 15$ nm, $a = 17.5$ nm, $\alpha = 16°$, and tip rounding radius s =3 nm. Light is coming from the left, with the electric field contained in the plane of the plots.

bright spots appear in the SAED pattern, clearly demonstrating the strong crystallinity, as well as the crisscrossing nature of the individual petals in the assembly, as similarly reported for Pt nanothorn assemblies [16]. The continuous fringe pattern observed in the HRTEM and the corresponding fast Fourier transform (FFT) image (figure 3(d)) elucidate the single crystalline nature of the individual tips. Remarkably, we have identified a common [011] growth direction for all analyzed tips, even from different particles, which is indicative of a higher surface energy for {110} facets, as compared with {111} and {100}, as expected for an fcc lattice [17]. The absence of twin planes in the individual tips illustrates the fact that, beyond aesthetics, the essence of these structures lies solely on the complex manifoldness of single crystalline tips. It should also be stressed that these complex nanostructures are extremely stable at room temperature, as confirmed by optical and microscopic characterization performed several months after synthesis.

PVP has been often used as a stabilizer for the synthesis of metal nanoparticles with various geometries, and has been claimed to play an important role in the anisotropic growth. However, only a few reports identify PVP as the main reducing agent [11, 16, 18], since it has been used in conjunction with external energy sources such as temperature, ultrasound, etc. In the present case, however, we found that PVP is the main element responsible for driving reduction under ambient conditions, and owing to the large PVP/Au molar ratio it promotes the formation of these exotic Au nanostructures with a high degree of shape control. As expected (see figures S3 and S4 (available at stacks.iop.org/Nano/19/015606)), the molecular weight of PVP does not have any drastic effect on the size/shape of the resultant Au nanostructures, other than those related to changing the number of monomeric units. The presence of preformed nanoparticle seeds and their surface restrained rapid growth along the [110] direction controls the formation of a number of petals/tips in the star/flower-like nanoassembly. Although we can argue at present that PVP plays a major role in the reduction kinetics and the final morphology (see figure 2), the precise formation mechanism requires a systematic study of the effect of various synthesis parameters such as the PVP/Au molar ratio and Au seed to metal ion ratio on the morphology of these nanostar assemblies, which is currently underway, and will be reported elsewhere.

Of major interest are the optical properties of these complex Au nanostructures. As previously reported for Pt nanothorns [16], the presence of a large number of sharp tips in our Au nanostars is expected to enhance SERS activity. Furthermore, despite the apparent irregular geometry, the extinction spectra of these nanostars in DMF show well-defined localized surface plasmon features (figure 4). A very intense absorbance band centered around 764 nm was measured for this sample, along with a less intense band/shoulder, centered around 550 nm, somehow resembling the usual spectra of (polydisperse) gold nanorods [2]. As discussed below, these bands are attributed to dipolar resonances, localized at either the tips or the central core of the particles. In terms of quantifying the precise optical response of these intricate Au nanostructures, optical modeling was carried out by means of the boundary element method (BEM) [9], which can be readily applied to objects with arbitrary shapes and axial symmetry [11].

For the present case of nanostars, we employed a geometrical model consisting of a central sphere with either one or two (located at opposite sides of the sphere) pseudo-conical caps (see inset in figure 4). The validity of this simplified model is confirmed by the results obtained, since the main difference arising from including an additional tip is an increase of the intensity ratio between the two characteristic absorption bands (see figure S5 in SI (available at stacks.iop.org/Nano/19/015606)), but only marginally affecting the resonance frequencies. This result confirms that the number of tips is of minor importance for determining the spectral position of the main, longitudinal resonance wavelength, while both the aperture angle (α)

and the roundness of the tip (s) are of major importance, since small changes lead to a significant shift in the main longitudinal resonance (see figure S6 in SI (available at stacks.iop.org/Nano/19/015606)). From the simulated extinction spectra (averaged over the distribution of angular tip apertures measured from TEM images, and with a tip defined by a 3 nm rounding radius) for spheres with one and two tips (figure 4), it can be clearly seen that the calculated spectra are in extremely good agreement with the experimental results, and it is further evidenced that the intensity of the low energy band is enhanced with respect to the high energy one for increasing number of tips, which explains the experimental result. Additionally, our BEM calculations demonstrate that plasmon oscillations confined within the tips give rise to the main plasmon band (see the near-field enhancement maps in figure 4) and dominate the overall optical response, over inter-tip interaction and dipolar oscillations confined within the core (550 nm wavelength). Since the enhanced electric field localized at the tips is the relevant parameter determining the SERS efficiency of metallic nanostructures, this result confirms that the presence of multiple tips should provide a largely enhanced efficiency for these novel nanostructures.

To complement these predictions, we have additionally explored the expected performance of our particles in SERS through BEM calculations of the Raman enhancement for axially symmetric particles with two tips and for different values of their geometrical parameters. The enhancement is averaged over random positions of the sampled molecule on the particle surface and over random orientations of the excitation and emission dipoles, thus representing a situation commonly encountered in practice, in which the particle is covered with a monolayer of molecules in a suspension that is then evaporated over a substrate. The Raman enhancement is the combined effect of the local increase in light intensity when the particle is illuminated with light at the resonance wavelength λ_{in} and the enhancement in the strength of the Raman dipole-emission transition at a longer wavelength λ_{out}. The signal is customarily represented as a function of the difference between the inverse of these two wavelengths (i.e., the Raman shift). We use the reciprocity theorem [19] to express the angle-averaged local-field enhancement of the incident light in terms of the enhancement in the emission of a randomly oriented dipole at the same wavelength, λ_{in}. This allows us to obtain the ratio between the Raman signal for molecules attached to the particle and the signal for free standing molecules (i.e., the SERS enhancement) as

$$\mathrm{SERS} = \frac{\int_{\mathrm{surface}} \mathrm{d}^2\mathbf{s}\,\Gamma(\lambda_{in})\Gamma(\lambda_{out})}{A\Gamma_0(\lambda_{in})\Gamma_0(\lambda_{out})},$$

where the integral is extended over the surface of the particle, A is the area of the latter, $\Gamma(\lambda)$ is the wavelength- and position-dependent emission rate of a dipole at the particle surface, and $\Gamma_0(\lambda)$ is the emission rate for the same dipole in air. Figure 5 shows the resulting enhancement for a particularly favorable choice of parameters, in which the tips are relatively sharp. Two prominent structures are observed, one at the tip resonance wavelength above 700 nm and a weaker one at the sphere-like resonance (500 nm). The former yields an enhancement of

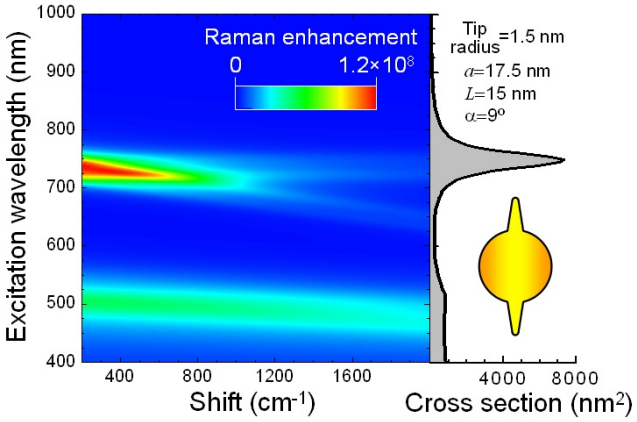

Figure 5. Left: calculated Raman enhancement in a two-tip gold particle in air. The transitions involved in the Raman process are assumed to occur 2 nm away from the gold surface. Right: scattering cross section of the same particle. The particle shape and geometrical parameters are shown in the insets.

10^8, which is rather high, considering the degree of control over the particle resonance. The sphere-like plasmon band produces an enhancement 2–3 times smaller, but still rather significant. Actually, when less sharp tips are considered (e.g., for tip radius of 3 nm and/or $\alpha = 16°$, maintaining the rest of the parameters unchanged), the tip-driven SERS is actually weaker than that produced by the sphere-like mode. This is in contrast to the scattering cross section, in which the tip-mode is always dominant because it is dictated by the induced dipole, favored by the increase in aspect ratio due to the tips, rather than by the averaged local fields that are relevant in SERS. Figure 5 shows results for uniform distributions of molecules over the particle surface, but enhancement factors approaching ten orders of magnitude are obtained for molecules absorbed preferentially near the tip. Similar enhancement factors have been predicted for molecules located at the gap between a particle dimer [20, 21], which is extremely difficult to control in practice. In our case, single particles controlled through colloidal chemistry yield similar effects, which suggests that nanostars are natural candidates for SERS applications. It should also be noted that the calculations were made for one particle with two tips, while our particles contain a large number of tips, and therefore a larger enhancement is to be expected.

4. Conclusions

In summary, star-like, multipod Au nanoparticles have been synthesized by seeded growth in a concentrated solution of PVP in DMF, with no need for any external energy sources. HRTEM images clearly reveal their interesting interlaced assembly as well as the single crystalline structure of the tips, a unique morphology very much suitable for exciting SERS applications. The optical response of these nanostructures was simulated by BEM calculations and found to be mainly confined within the tips. We have additionally shown theoretical prediction of the expected SERS efficiency of these particles, while experimental demonstration will be reported elsewhere. Further work is in progress to understand

the precise formation mechanism of these assemblies and the effect of external parameters such as temperature, solvent, PVP molecular weight, and morphology of preformed nanoparticle seeds.

Acknowledgments

Funding from the Spanish Ministerio de Educación y Ciencia is acknowledged in the form of a fellowship (PSK) and Grants MAT2004-02991 and NAN2004-08843-C03/C05.

References

[1] Burda C, Chen X, Narayanan R and El-Sayed M A 2005 *Chem. Rev.* **105** 1025 and references therein
[2] Liz-Marzán L M 2006 *Langmuir* **22** 32 and references therein
[3] Hao F, Nehl C L, Hafner J H and Nordlander P 2007 *Nano Lett.* **7** 729
[4] Hao E, Bailey R C, Schatz G C, Hupp J T and Li S 2004 *Nano Lett.* **4** 327
[5] Krichevski O and Markovich G 2007 *Langmuir* **23** 1496
[6] Sau T K and Murphy C J 2004 *J. Am. Chem. Soc.* **126** 8648
[7] Burt J L, Elechiguerra J L, Reyes-Gasga J, Montejano-Carrizales J M and Jose-Yacaman M 2005 *J. Cryst. Growth* **285** 681
[8] Graf C, Vossen D L J, Imhof A and van Blaaderen A 2003 *Langmuir* **19** 6693
[9] García de Abajo F J and Howie A 2002 *Phys. Rev.* B **65** 115418
[10] Johnson P B and Christy R W 1972 *Phys. Rev.* B **6** 4370
[11] Sánchez-Iglesias A, Pastoriza-Santos I, Pérez-Juste J, Rodríguez-González B, García de Abajo F J and Liz-Marzán L M 2006 *Adv. Mater.* **18** 2529
[12] Pastoriza-Santos I and Liz-Marzán L M 1999 *Langmuir* **15** 948
Pastoriza-Santos I and Liz-Marzán L M 2002 *Nano Lett.* **2** 903
Pastoriza-Santos I and Liz-Marzán L M 2002 *Langmuir* **18** 2888
[13] Tsuji M, Hashimoto M, Nishizawa Y, Kubokawa M and Tsuji T 2005 *Chem. Eur. J.* **11** 440
[14] Nehl C L, Hongwei L and Hafner J H 2006 *Nano Lett.* **6** 683
[15] Xiong Y, Washio I, Chen J, Cai H, Li Z-Y and Xia Y 2006 *Langmuir* **22** 8563
[16] Tian N, Zhou Z-Y, Sun S-G, Cui L, Ren B and Tian Z-Q 2006 *Chem. Commun.* 4090
[17] Wang Z L 2000 *J. Phys. Chem.* B **104** 1153
[18] Hoppe C E, Lazzari M, Pardinas-Blanco I and Lopez-Quintela M A 2006 *Langmuir* **22** 7027
[19] Landau L D and Lifshitz E M 1960 *Electrodynamics of Continuous Media* (Reading, MA: Addison-Wesley)
[20] Xu H, Bjerneld E J, Käll M and Börjesson L 1999 *Phys. Rev. Lett.* **83** 4357
[21] Johansson P, Xu H and Käll M 2005 *Phys. Rev.* B **72** 035427

Supporting Information

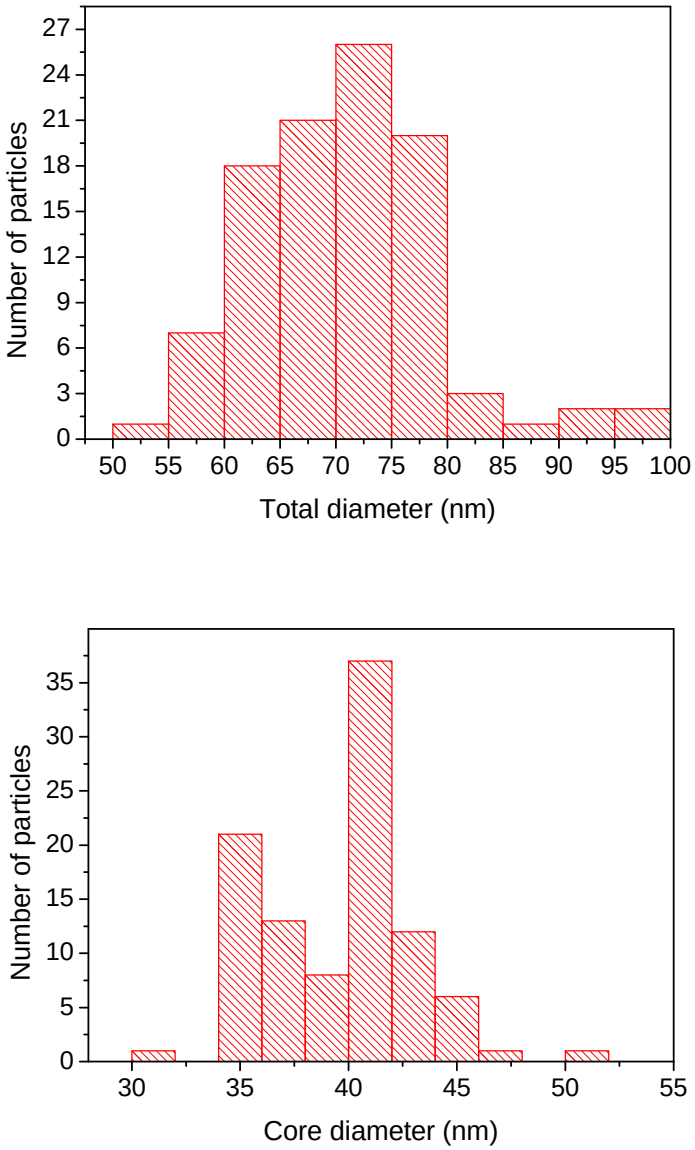

Figure S1. Histograms of total particle size (top) and core diameter (bottom) of Au nanostars synthesized using PVP (MW-24,000) 5 mM in DMF. A Gaussian fit to the total diameter distribution yields a value of 69.0±7.9 nm, and for the core 39.2±3.2 nm.

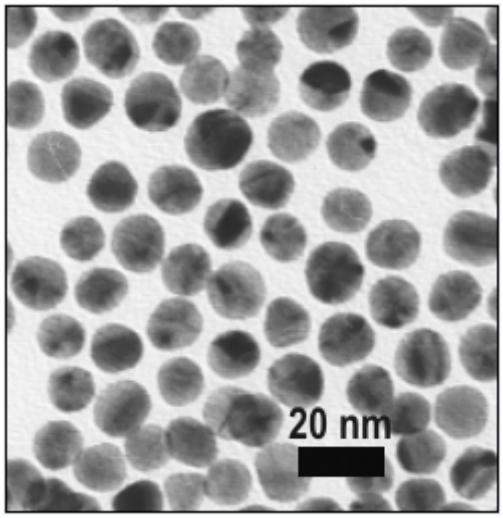

Figure S2. TEM image of PVP-capped Au nanoparticles used as seeds for the growth of nanostars.

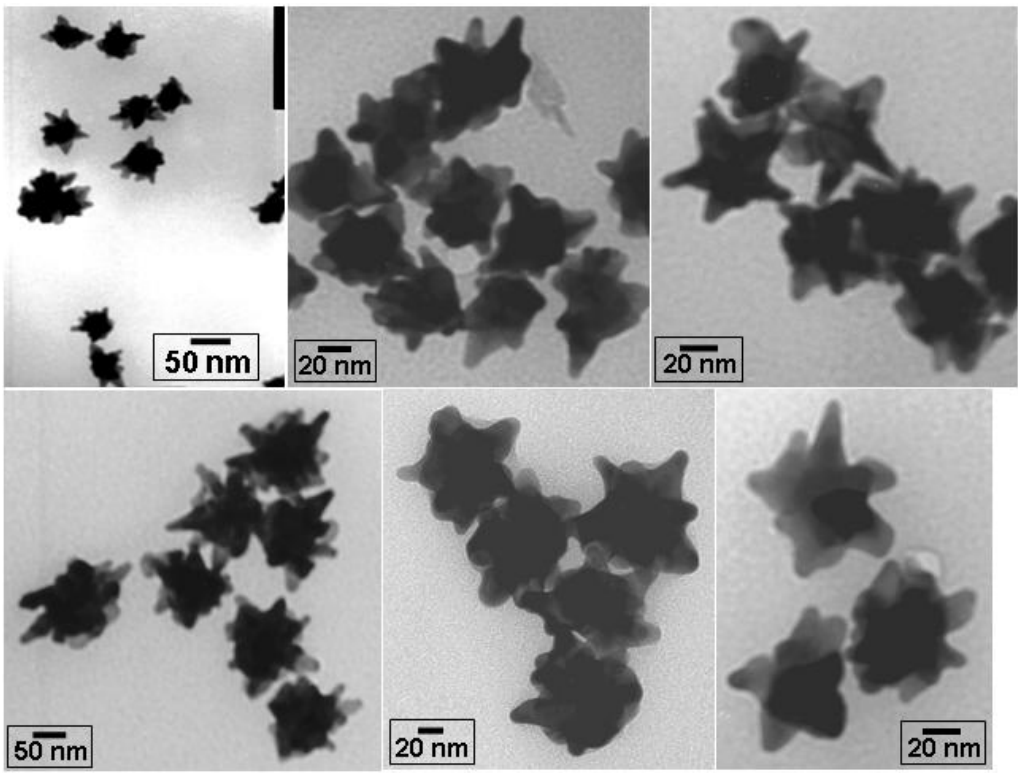

Figure S3. Representative TEM images (at various magnifications) of Au nanostars synthesized using PVP (MW-10,000) [Top: 10mM; Bottom: 5mM] in DMF for the same concentration of $HAuCl_4$ and Au seeds.

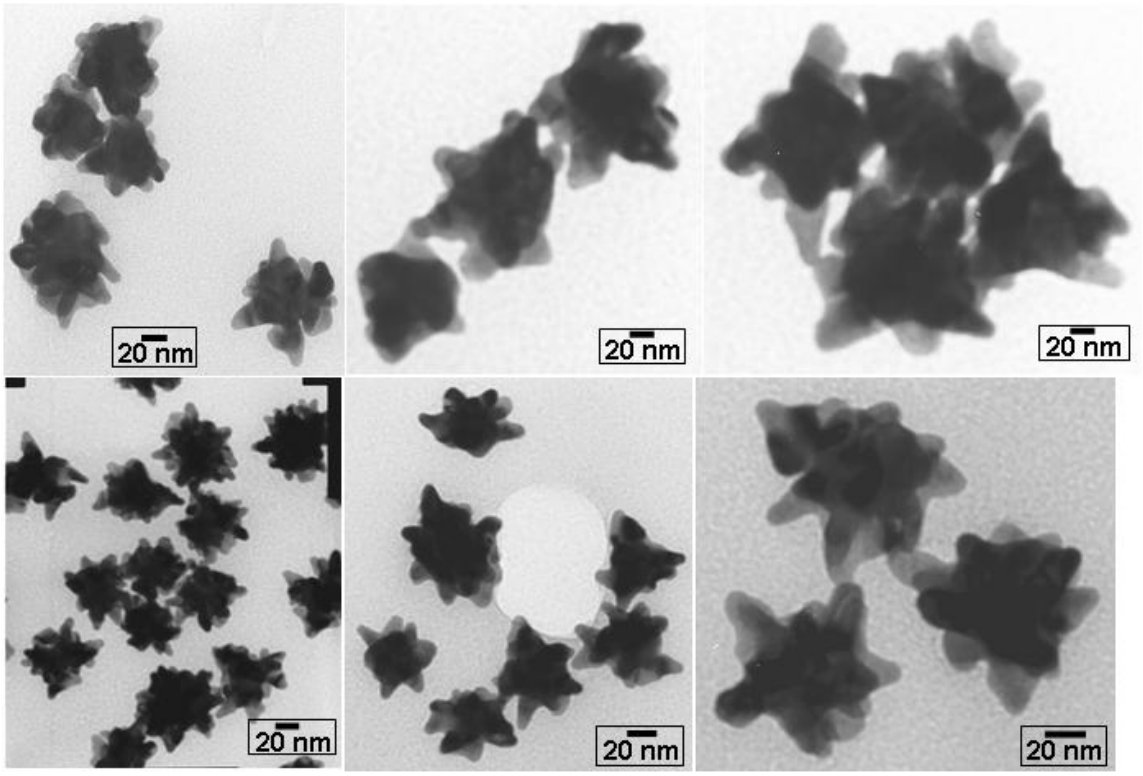

Figure S4. Representative low and high magnification TEM images of Au nanostars synthesized using PVP (MW-24,000) [Top, 10mM: Bottom, 5mM] in DMF for the same concentration of $HAuCl_4$ and the Au seeds.

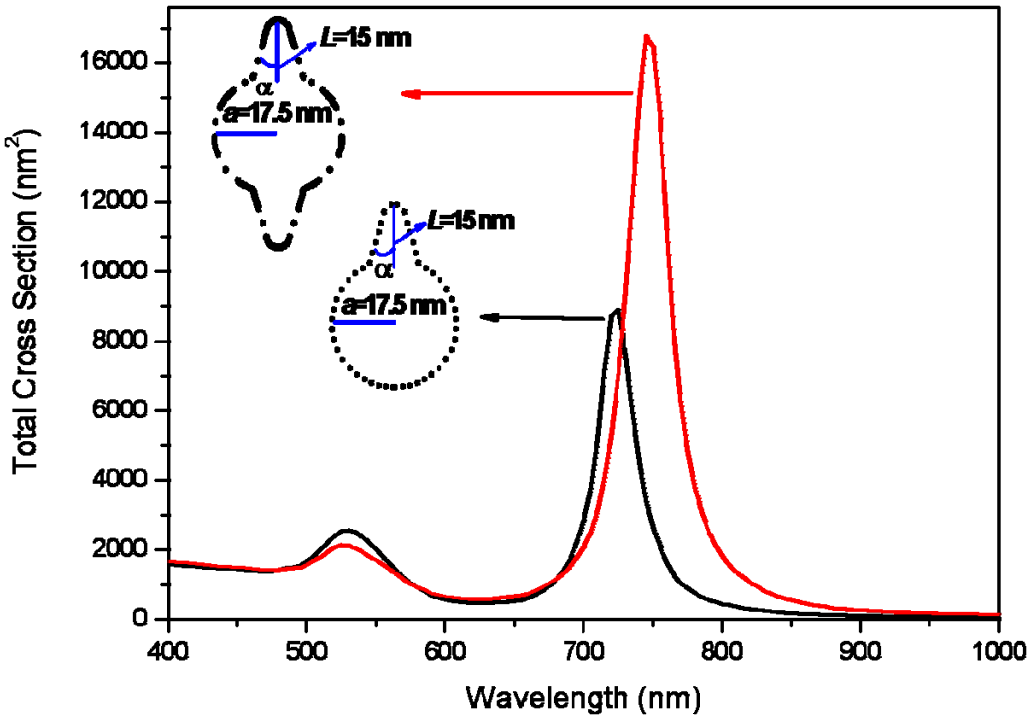

Figure S5. Calculated spectra for a sphere with one (black) and two (red) tips. The dimensions used for the simulations were L=15 nm, a= 17.5 nm, =16º, and tip-rounding radius s=3 nm.

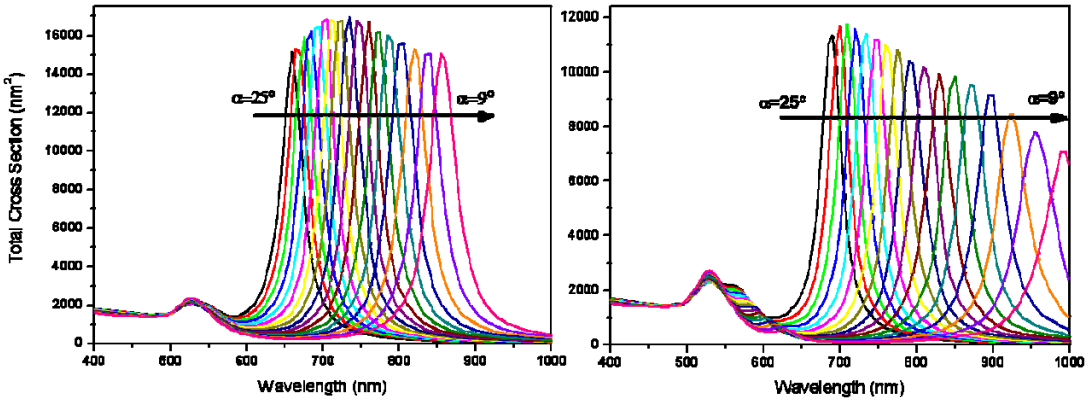

Figure S6. Calculated spectra at different aperture angles for a sphere with two tips. The dimensions used for the simulations were L=15 nm, a= 17.5 nm, and tip-rounding radius 3 nm (left) and 1.5 nm (right). Each individual spectrum is much narrower than the experimental one shown in the main paper (Figure 3, left panel), mainly due to finite size distribution of tip-aperture angles in the synthesized particles, which is taken into account in the -averaged calculations presented in Figure 3 (broken curves).